Supplemental material for manuscript:

A Unified Structural Model of the Mammalian Translocator Protein (TSPO)

Yan Xia[1,2], Kaitlyn Ledwitch[1,2], Georg Kuenze[1,2], Amanda Duran[1,2], Jun Li[3], Chuck Sanders[4], Charles Manning[3], Jens Meiler[1,2*]

[1]Center for Structural Biology, Vanderbilt University, Nashville, TN 37240, USA
[2]Department of Chemistry, Vanderbilt University, Nashville, TN 37235, USA
[3]Institute of Imaging Science, Vanderbilt University, Nashville, TN 37232, USA
[4]Department of Biochemistry, Vanderbilt University, Nashville, TN 37240, USA

*To whom the correspondence should be addressed: Jens Meiler, Department of Chemistry, Vanderbilt University, Center for Structural Biology, MRBIII 5144B, Nashville, TN 37232. Telephone: (615) 936-5662. Fax: (615) 936-2211. E-mail: jens.meiler@vanderbilt.edu

Table of Contents

Supporting Figures

Figure S1. *Bound conformation and interactions of PK11195 in experimental TSPO structures.*

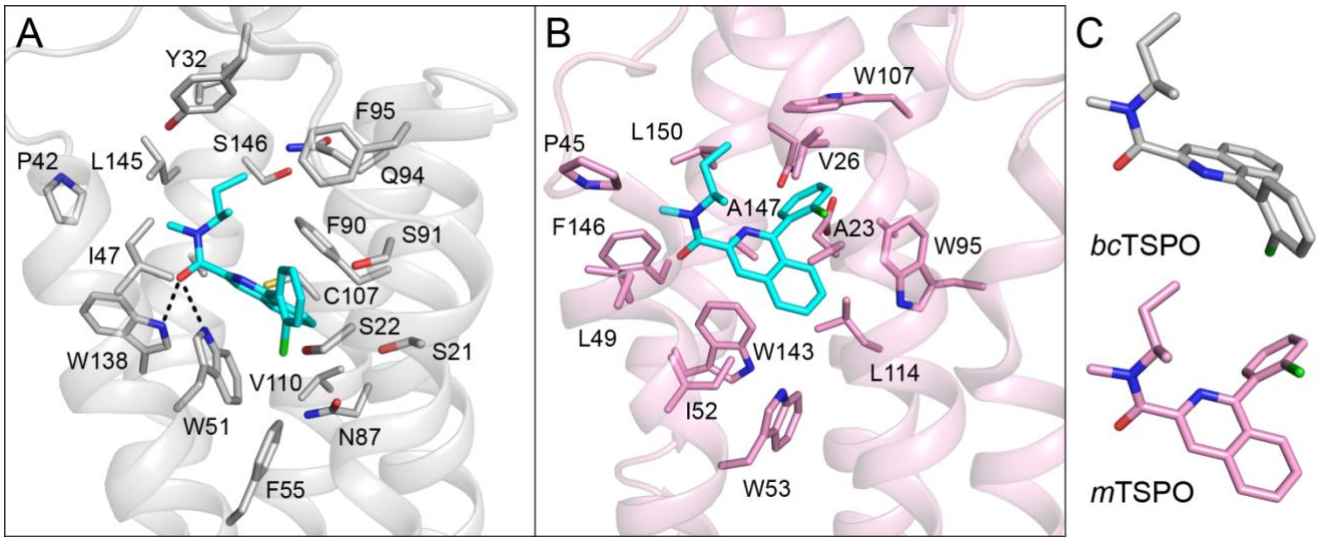

Figure S1. *Bound conformation and interactions of PK11195 in experimental TSPO structures.* PK11195 binding mode in (A) the *bc*TSPO X-ray crystal structure (PDB ID: 4RYI) and (B) the *m*TSPO NMR structure (PDB ID: 2MGY). The PK11195 ligand (cyan) and the side-chains of residues in the binding pocket are depicted as sticks. Amino acid residues are labeled with their one-letter code and position in the *m*TSPO or *bc*TSPO sequence, respectively. Potential polar contacts between the carbonyl group in PK11195 and the side-chains of W51 and W138 in *bc*TSPO are indicated by dashed lines. (C) Bound conformation of PK11195 in *bc*TSPO (top) and *m*TSPO (bottom). For ease of comparison, PK11195 conformers were superimposed onto their butan-2-yl-carboxamide group. Note that the 2-chlorophenyl-N-methylisoquinoline group is flipped by ~150° between the *m*TSPO- and *bc*TSPO-bound conformation.

Figure S2. *Purification and fluorescence measurement of mTSPO.*

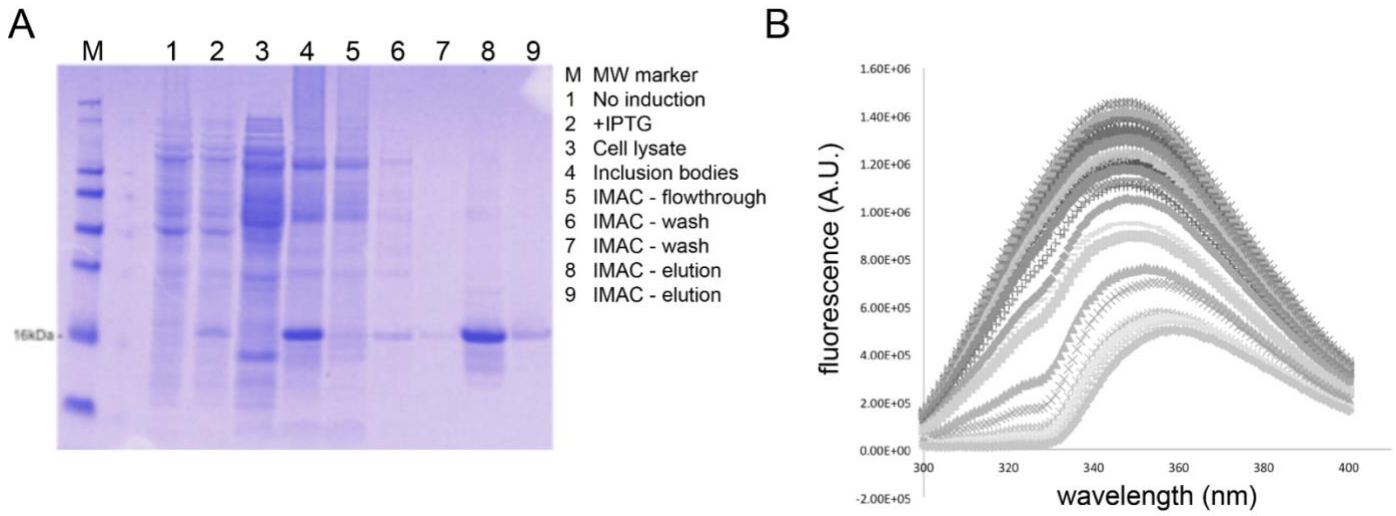

Figure S2. *Purification and fluorescence measurement of mTSPO*. (A) SDS-PAGE analysis of samples taken at steps during the purification of *m*TSPO. Protein purity was estimated to be at least 95%. (B) Tryptophan fluorescence spectra of *m*TSPO during titration of *m*TSPO with PK11195. Tryptophan fluorescence was not completely quenched even at high ligand concentrations.

Figure S3. *Characterization of PK11195 binding to mTSPO under different detergent concentrations and temperature conditions by intrinsic tryptophan fluorescence.*

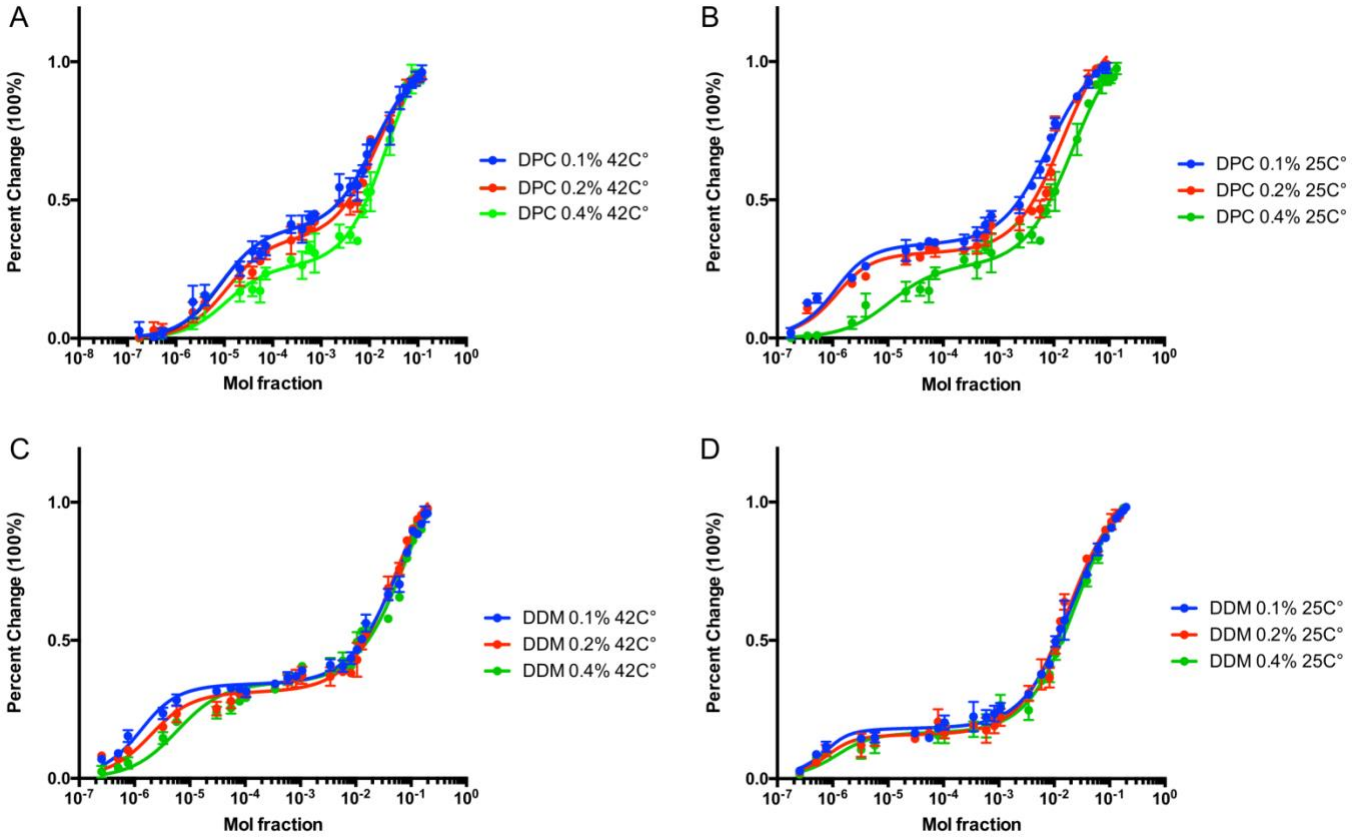

Figure S3. *Characterization of PK11195 binding to mTSPO under different detergent concentrations and temperature conditions by intrinsic tryptophan fluorescence.* The x-axis is plotted as log mole fraction units and the y-axis is plotted as percent maximal change to allow for direct comparison between different detergent concentrations. (A) Fluorescence quenching for PK11195 and *m*TSPO in 0.1% (w/v) DPC, 0.2% (w/v) DPC, 0.4% (w/v) DPC at 42C° and (B) at 25C°. (C) Fluorescence quenching for PK11195 and *m*TSPO in 0.1% (w/v) DDM, 0.2% (w/v) DDM, 0.4% (w/v) DDM at 42C° and (D) at 25C°. The average and standard deviations are represented as points and bars, respectively, and reflect at least three independent experiments. See methods for fitting procedure.

Figure S4. *NOE distance deviations and Pro-Pro backbone conformations of mTSPO$^{NMR\text{-}opt}$ structure and mTSPO^{RosettaCM} model.*

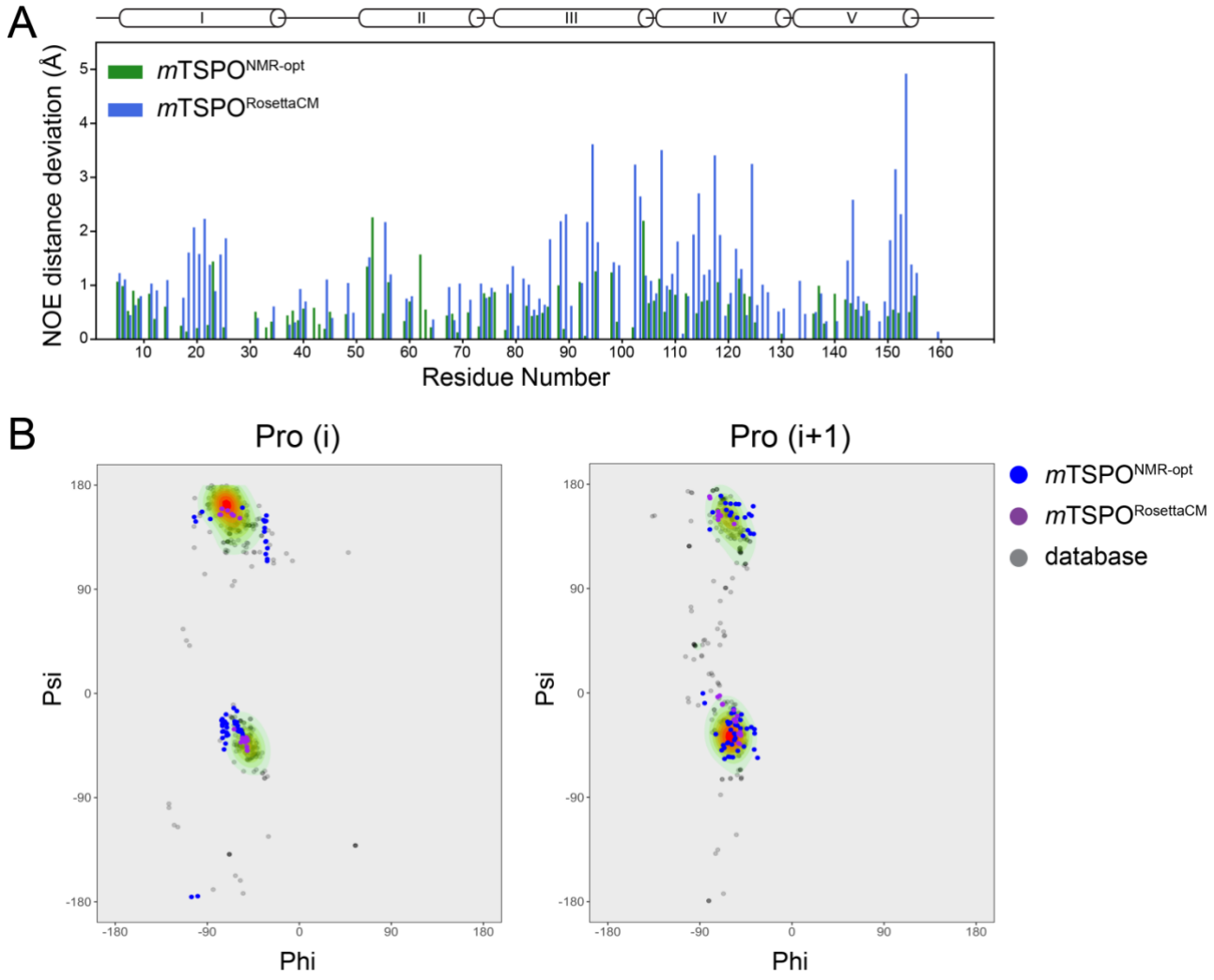

Figure S4. *NOE distance deviations and Pro-Pro backbone conformations of mTSPO$^{NMR\text{-}opt}$ structure and mTSPO^{RosettaCM} model*. (A) The average per-residue NOE distance deviation (Å) is plotted against the *m*TSPO amino acid sequence. Helical regions are outlined above the plot. The per-residue NOE distance deviation was calculated by normalizing the sum of distance deviations of each residue by its number of NOE contacts. (B) Ramachandran diagram of Pro(i)-Pro(i+1) motifs. The φ/ψ angles of residue pairs Pro^{44}-Pro^{45}, Pro^{96}-Pro^{97} and Pro^{131}-Pro^{132} in *m*TSPO$^{NMR\text{-}opt}$ (blue points) and *m*TSPO^{RosettaCM} (purple points) are compared to database values (gray). The database was created from all Pro-Pro motifs in transmembrane regions of available membrane protein structures found in the PDB.

Figure S5. *2D ^{1}H-^{15}N TROSY-HSQC spectra of mTSPO reconstituted in DPC micelles in the presence of 5.0 mM VUIIS8310 and 5.0 mM PK11195.*

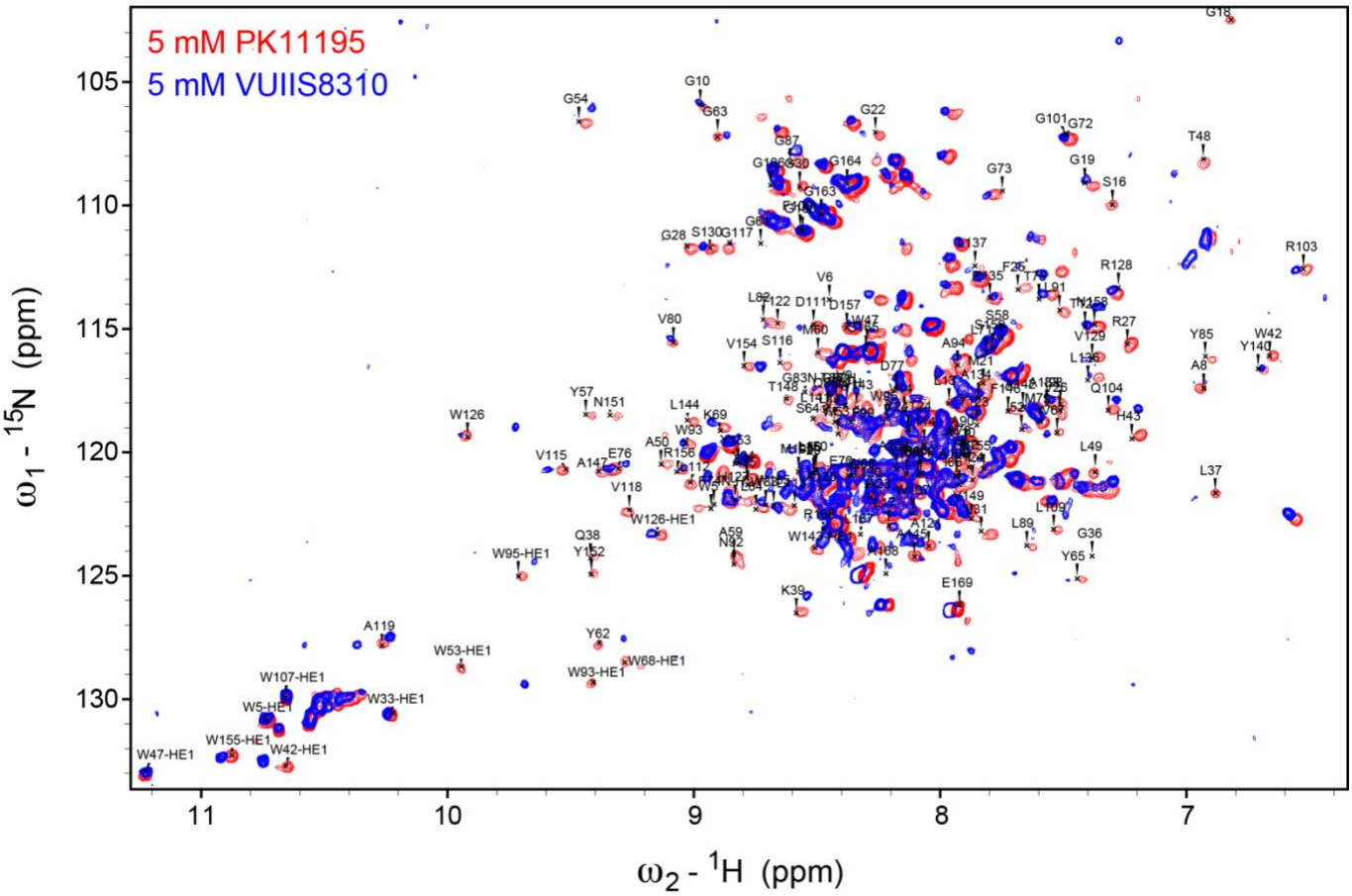

Figure S5. *2D ^{1}H-^{15}N TROSY-HSQC spectra of mTSPO reconstituted in DPC micelles in the presence of 5.0 mM VUIIS8310 and 5.0 mM PK11195.*

Figure S6. *Docking of PK11195 and VUIIS8310 ligands to mTSPO and bcTSPO models.*

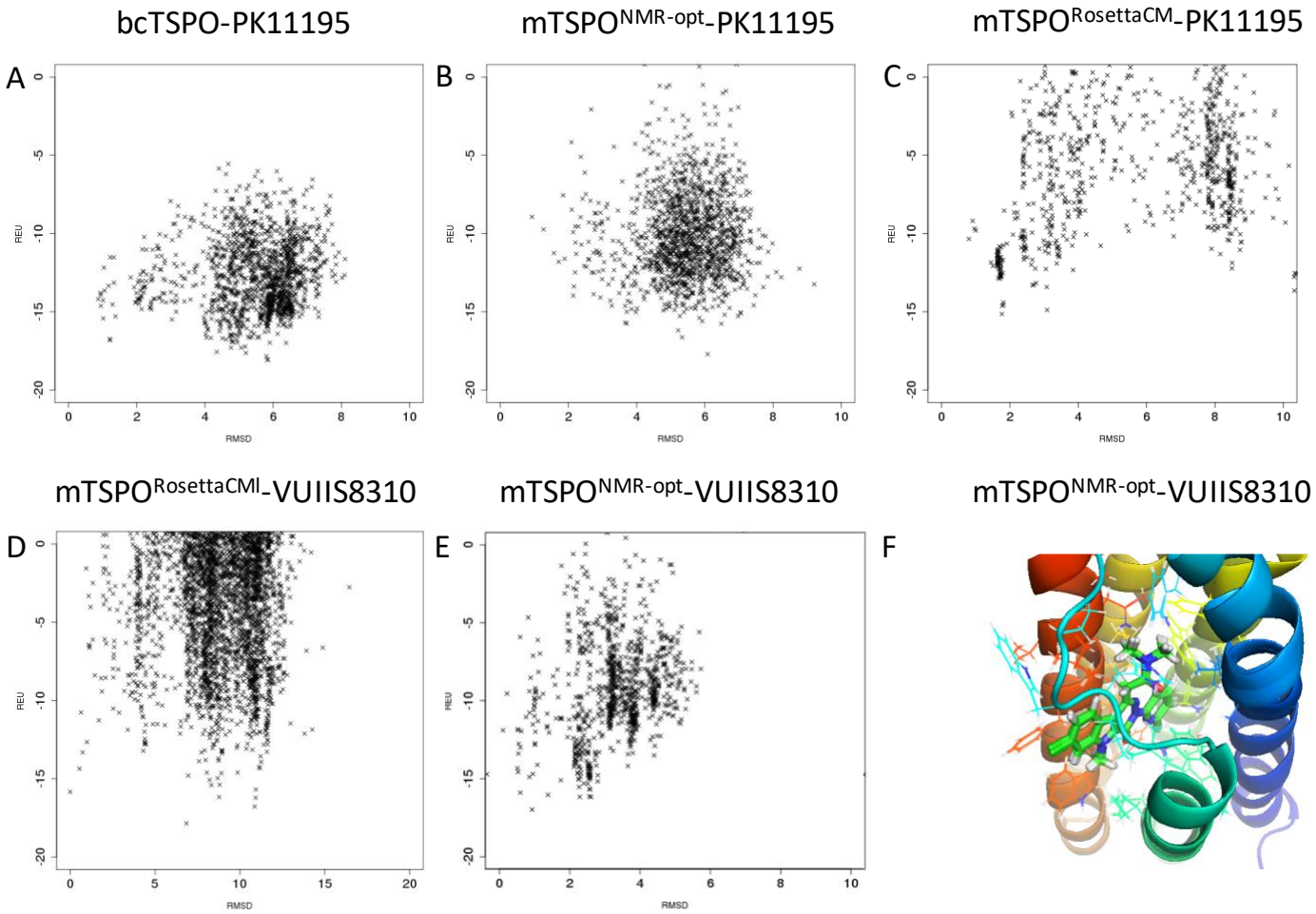

Figure S6. *Docking of PK11195 and VUIIS8310 ligands to mTSPO and bcTSPO models.* For each protein model and ligand, the Rosetta binding energy (in REU) is plotted vs. the ligand's RMSD (in Å) (without superimposition) relative to the experimental structure (for *bc*TSPO$^{X\text{-}ray}$ and *m*TSPO$^{NMR\text{-}opt}$) or the lowest-energy docking model (*m*TSPO^{RosettaCM}), respectively. The funnel-likeness of the energy-vs-RMSD plot is inspected to assess calculation convergence. Lowest-energy docking models are displayed in Figure S8 and compared to the experimental structure where available. (A) PK11195 docked to *bc*TSPO$^{X\text{-}ray}$. (B) PK11195 docked to *m*TSPO$^{NMR\text{-}opt}$. (C) PK11195 docked to *m*TSPO^{RosettaCM}. (D) VUIIS8310 docked to *m*TSPO^{RosettaCM}. (E) VUIIS8310 docked to *m*TSPO$^{NMR\text{-}opt}$. Docking of VUIIS8310 to *m*TSPO^{RosettaCM} yielded two low-energy clusters. Models from the larger cluster at high RMSD values were found to be in better agreement with the chemical shift perturbation data, and the lowest-energy model from that cluster was selected as representative model (shown in Figure 7 in the main text). Docking of VUIIS8310 to *m*TSPO$^{NMR\text{-}opt}$ yielded two low-energy ligand binding models that are shown in panel (F). The observed binding mode characterized by VUIIS8310 protruding into the membrane and lacking protein burial was found inconsistent with the chemical shift perturbation data.

Figure S7. *Binding pose location of the PK11195 ligand and the VUIIS8310 ligand bound to mTSPO compared against experimentally-derived structures and Rosetta models.*

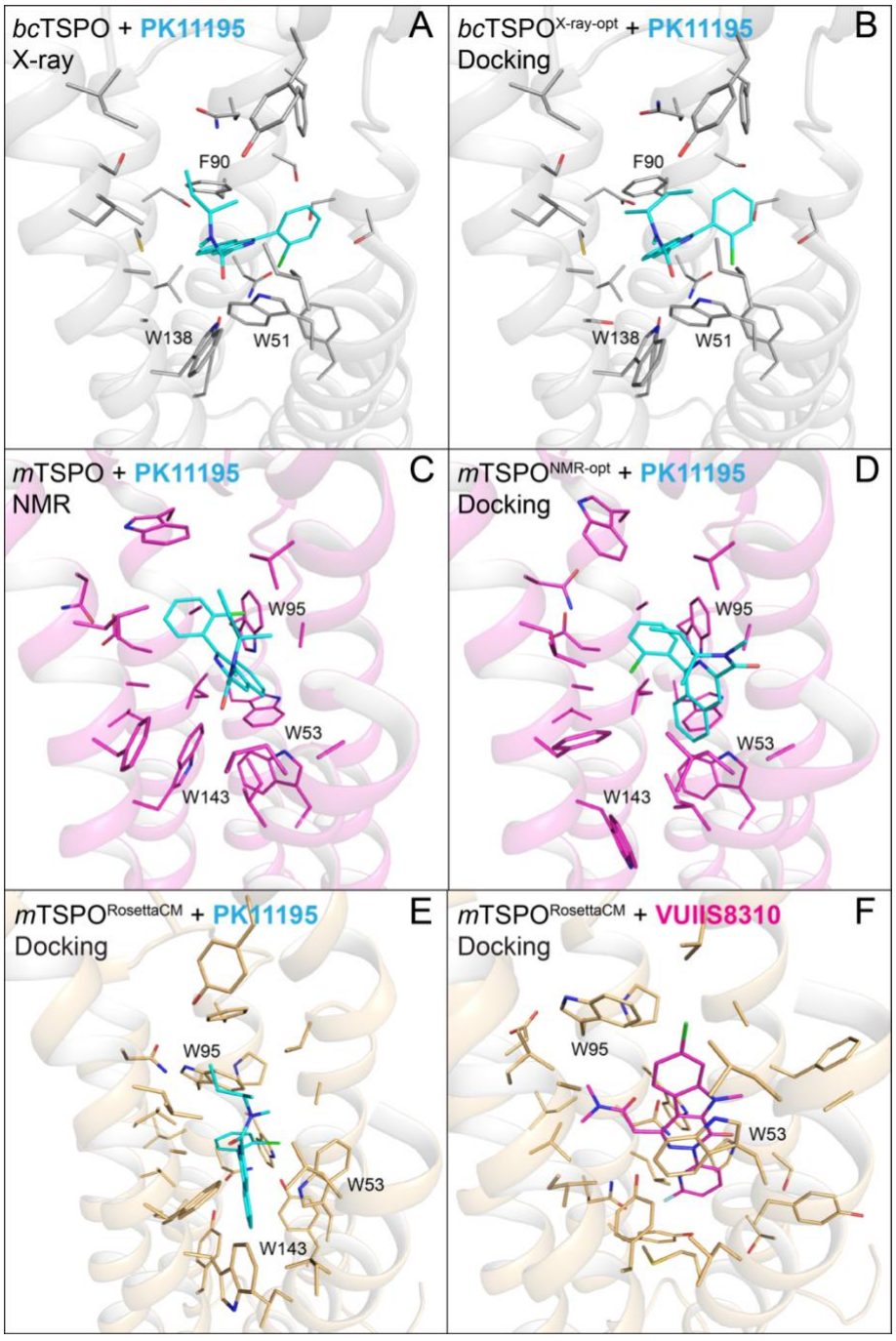

Figure S7. *Binding pose location of the PK11195 ligand and the VUIIS8310 ligand bound to mTSPO compared against experimentally-derived structures and Rosetta models*. (A) The X-ray crystal structure of PK11195 bound to *bc*TSPO. (B) PK11195 docked to the X-ray crystal structure of *bc*TSPO after energy minimization in Rosetta. (C) The NMR solution structure of PK11195 bound to *m*TSPO. (D) PK11195 docked to the energy-minimized *m*TSPO$^{\text{NMR-opt}}$ model. (E) PK11195 docked to the *m*TSPO$^{\text{RosettaCM}}$ model. (F) VUIIS8310 docked to the *m*TSPO$^{\text{RosettaCM}}$ model. Ligand docking leveraged the energy-minimized structures of *bc*TSPO$^{\text{X-ray}}$ and *m*TSPO$^{\text{NMR}}$, and the *m*TSPO$^{\text{RosettaCM}}$ homology model constructed from multiple templates.

Supporting Tables

Table S1. *Apparent binding constant of PK11195 to mTSPO in various conditions*.

Sample	K_{app}^{Tr1}	K_{app}^{Tr2}	K_{app}
DPC 0.1% 25°C	5.79E-07	8.30E-03	
DPC 0.2% 25°C	6.33E-07	1.46E-02	
DPC 0.4% 25°C	1.05E-05	2.19E-02	
DPC 0.1% 42°C	8.39E-06	1.23E-02	
DPC 0.2% 42°C	5.60E-06	6.87E-03	
DPC 0.4% 42°C	2.66E-06	5.47E-03	
DDM 0.1% 42°C	7.62E-07	7.85E-01	
DDM 0.2% 42°C	1.45E-06	8.66E-01	
DDM 0.4% 42°C	5.42E-06	8.60E-01	
NMR 42°C			>5.74E-03
The values reported in the table are all in mol fraction units. The fluorescence binding data were fitted with equation 3 to report K_{app}^{Tr1} and K_{app}^{Tr2} with prior assumption of a high affinity binding event. The NMR binding experiment data was fitted with equation 5 to report a lower limit of K_{app} for apparent binding constant.			